
PatchNet: Unsupervised Object Discovery based on Patch Embedding

Hankyu Moon¹, Heng Hao², Sima Didari³, Jae Oh Woo⁴, and Patrick Bangert⁵

^{1,2,3,4,5}Samsung SDS Research America
{hankyu.m,h.heng,s.didari.jaeoh.w,p.bangert}@samsung.com

Abstract

We demonstrate that frequently appearing objects can be discovered by training randomly sampled patches from a small number of images (100 to 200) by self-supervision. Key to this approach is the *pattern space*, a latent space of patterns that represents all possible sub-images of the given image data. The distance structure in the pattern space captures the co-occurrence of patterns due to the frequent objects. The pattern space embedding is learned by minimizing the contrastive loss between randomly generated adjacent patches. To prevent the embedding from learning the background, we modulate the contrastive loss by color-based object saliency and background dissimilarity. The learned distance structure serves as *object memory*, and the frequent objects are simply discovered by clustering the pattern vectors from the random patches sampled for inference. Our image representation based on image patches naturally handles the position and scale invariance property that is crucial to multi-object discovery. The method has been proven surprisingly effective, and successfully applied to finding multiple human faces and bodies from natural images.

1 Introduction

The main challenge of object detection stems from (1) the variations of location, size, and pose of objects, (2) the occurrence of multiple objects in the same scene with possible occlusions, and (3) the infinite diversity of backgrounds. Modern CNN technology is capable of handling these challenges by its design of convolutional architecture that enables position and scale invariance and by fitting millions of neural network parameters. Both the network architectures and the sheer number of trainable parameters provide enough capacity to identify objects under diverse scene contexts and imaging conditions. The current state of the art object detection approaches employ either ‘proposal’ based [25] or ‘one shot’ based [16, 12] approaches over deep features learned by CNNs. They are quite capable of finding objects and classifying them into hundreds or even thousands of categories.

Despite the progresses and their real-world utility, there is a major limitation with the current approaches: training a CNN for object detection requires a large number of images with object boundaries manually marked. This common limitation naturally motivates the needs for ‘unsupervised’ or ‘semi-supervised’ frameworks. There have been recent developments in unsupervised image representation learning and clustering that show promises toward unsupervised classification. Most notably, deep clustering based on pre-text training [9, 21] is approaching classification accuracy closer to the supervised state of art. This class of approaches is able to find clusters of images that can map to one of the specified object categories without supervision. This is enabled by the combination of clustering in neural embedded feature space, and self-supervised contrastive learning that constrains the embedding. Despite their surprising effectiveness toward classification tasks, the deep clustering

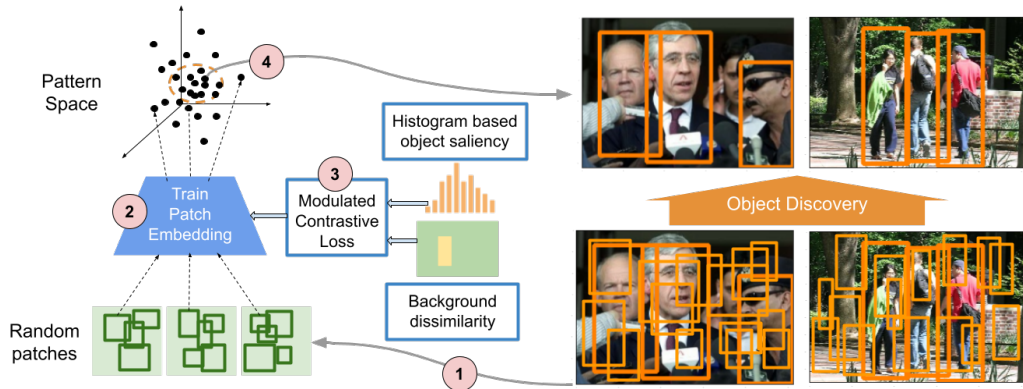


Figure 1: Overall scheme of the approach

approach in its current form is not applicable to detection problems due to the unconstrained range of possible object scales and positions.

For this type of unsupervised approach to be effective, each image should have a single object properly cropped so that it is close to the image center and with limited size variations. This conventional idea of ‘an object as a vector’ inherently lacks the key ability to (1) represent multiple objects (while preserving their locations and sizes) in the image, and at the same time (2) extract out these objects into a common mathematical representation with which they can be compared and analyzed. The second condition clearly requires the objects to be aligned. This is especially critical because misalignment in both position and scale incurs highly nonlinear changes in pixel space. Obviously, availability of tight bounding boxes around each object will satisfy these two key requirements. Under the unsupervised scenario, however, this is essentially a chicken-and-egg problem.

In our proposed work, we utilize a patch-based image representation that fulfills the critical needs toward unsupervised object finding mentioned above. The patches sample all possible sub-images in a given image set, and are capable of capturing any number of objects. We combine self-supervised training with object saliency constraints that learns the mapping from the set of all sub-images to a common latent space. The learned mapping is tuned to patterns that frequently appear in the image set, and sends these patterns to a tight cluster. This self-emergent structure in the pattern space corresponds to the frequently appearing objects. Figure 1 illustrates our overall scheme with numbered items below point to the circled numbers in the figure:

1. Image patches sampled at random locations and scales over an image set,
2. A neural embedding of these patches into a *pattern space* learned by contrastive training,
3. *Objectness* constraints by modulating the contrastive loss during training, so that the learned embedding is sensitive to object saliency while suppressing the background patterns commonly occurring in the image set, and
4. An unsupervised clustering step that identifies the frequently appearing objects in the images that leads to object discovery.

Our approach is completely label-free because our embedding network is trained from random weights. We primarily show applications to the problem of person detection. This is in contrast with the existing Object Discovery work [6, 23, 24] that shows success in discovering objects such as airplanes, cars, animals having typical color/texture and appearing against simple backgrounds (sky, pavement, grass, etc.). These proposal based approaches suffer from the *part domination* issue when applied to human detection due to diversity in clothing and background. We show that our approach is able to train a convolutional encoder network with a very small number of images (200 or less) and discover human bodies and faces at high success rates. We suspect this is due to the highly efficient patch based image representation that learns the *building blocks* of objects, in contrast to the whole-image based approaches that require a larger number of images to learn diverse object instances under differing imaging conditions.

2 Related work

Several approaches have emerged for object detection that require fewer ground truth bounding boxes or only image-level labels such as semi-supervised, weakly-supervised, and object colocalization models. Multiple Instance Learning (MIL) [1] and its modified variations are one of the main approaches developed for weakly supervised problems. MIL assumes that each image consists of multiple instances or bags of regions. A bag is called positive if it contains an object and MILs models try to find regions in the positive bags. Several studies were conducted to improve the performance of MIL approaches by enhancing the region proposal part, increasing the robustness of optimization, solving part domination issues, and memory efficiency [17]. Attention and recurrent modules were developed and integrated with MILs to refine the region proposal selection tasks which were originally based on standard proposal generation methods such as selective search [18, 19, 11]. Weakly supervised or semi-supervised models require the training of a subset of training data with class level information. To alleviate the need for classification annotation of the training dataset, the colocalization methods bring us one step closer to the fully unsupervised learning. In these approaches either a pretrained CNN model (on classification tasks) or an off-the-shelf region proposal model is used to localize and detect the objects. Cho et al [6] proposed a two-part colocalization model consisting of a region proposal matching and object localization steps. Randomized Prim’s algorithm [14] generates proposal regions. Then region pairs are compared and ranked by Probabilistic Hough Matching (PHM) algorithm. To further improve the performance of the aforementioned approach [6] Vo et al [23] introduced a graph representation for capturing the similarity of the image pairs and formulated as a graph optimization problem. They also leveraged features learned from a pretrained CNN model [24] for region proposal. These modifications lead to better performance for capturing multiple objects.

In a departure from two-part localization methods MONet[2], IODINE [8] and GENESIS [7] models were developed that decomposed scenes into objects using sets of latent variables for an object-based representations. To further improve these set-structured based object discovery models [13] proposed a Slot Attention module that learns the set-structured latent space. It was assumed that each set element corresponds to an object within the image. Hence, feeding learned features from a pretrained CNN model to the Slot Attention module coupled with a decoder, the objects can be localized and detected. Wei et al [26] proposed Deep Descriptor Transformation (DDT) that used the correlation between the features learned by a pretrained CNN network for the images in dataset. Rambhatla et al [15] proposed a dual memory model that uses the prior knowledge gained from detection of labeled categories to discover the unseen categories in a new unlabeled set. Zhang [27] proposed the Object Location Mining (OLM) model. OLM used feature representation of pretrained CNNs and salient pattern mining for object localization. The activation map generated by a pretrained CNN model (such as VGG-16) for each feature maps was used as an indicator to object existence. By extracting the activation maps and their connectivity and frequency, the salient objects were discovered. Our patch based representation and training is unique in the sense that it is purely unsupervised and does not depend on any object proposal, either neural network based [14] or deterministic feature based [20]. To the best of our knowledge, there have not been any other successful approaches that are able to discover multiple pedestrians from complex scenes.

3 Patch space representation

The patch based image representation satisfies the following properties, leading to unsupervised object discovery: (1) sampled image patches at multiple image positions and scales naturally satisfies position and scale invariance, (2) the learned association between the patterns from neighboring patches captures common object signatures, and (3) the patch based image representation is more efficient in the sense that it captures local features that are common to objects of the same or different classes. The existing approach of representing the whole object using a single bounding box and learning these instances in the whole image requires a very large number of samples.

Patches are sampled from an image frame at random positions and scales. The ranges of the size and aspect ratio (height divided by width) of the patches are determined such that the patches can capture objects having different scales and aspect ratios. The scale and aspect ratio of each patch are uniformly sampled from these ranges: $[\text{scale}_{\min}, \text{scale}_{\max}]$ and $[\text{ratio}_{\min}, \text{ratio}_{\max}]$. (Scale sampling scheme here and details in the Appendix) In our experiments, the scale range is fixed at [20, 256] for images scaled to width = 256. The aspect ratio range is a hyper-parameter and prior knowledge about

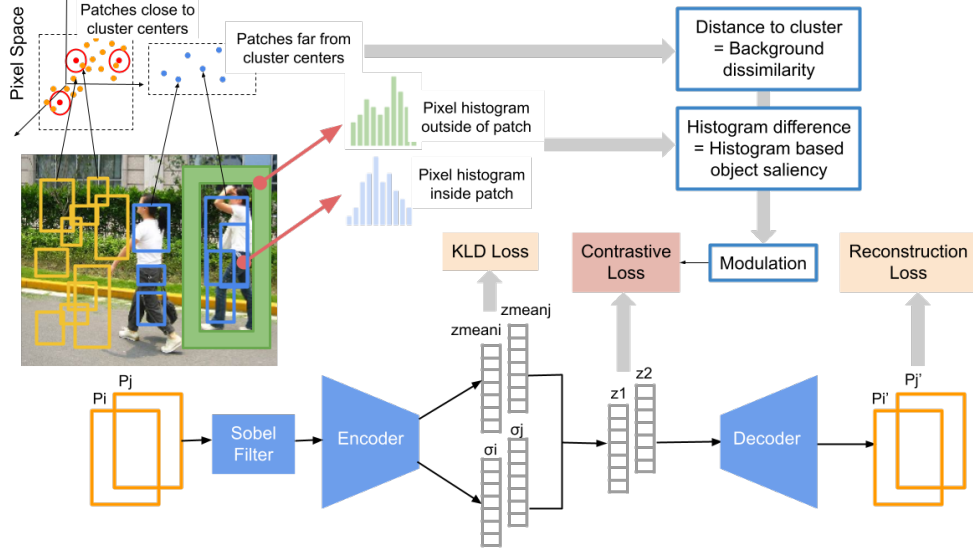


Figure 2: Training architecture and contrastive loss modulation

object shape is used. We found that the aspect ratio of $\text{ratio}_{\min} = \text{ratio}_{\max} = 3.0$ for person discovery and $1.67 - 2.0$ for face + upper body discovery are found suitable. The patches are generated in pairs so that the local pattern association can be learned during training; each pair is generated so that the two patches overlap (high Intersection over Union). More specifically, pairs of patches (p_1^i, p_2^i) , $i = 1, \dots, B$ are sampled as an input batch (of size B) such that $\text{IoU}(p_1^i, p_2^i) > 0.75$.

4 Patch embedding

The sampled patches are mapped to high-dimensional pattern vectors such that (1) each vector encodes the pattern information inside the patch and (2) the pairwise distance between the vectors reflects the co-occurrence of the corresponding patterns in natural images. The second property is enforced by the self-supervised training with a contrastive loss. The contrastive loss attracts adjacent pairs of patches together in the mapped latent space, while pushing unrelated pairs apart. At the end, the large number of embedded patches sampled from the image are endowed with a local distance structure. This is a 3D manifold of 2D position and scale in the high dimensional latent space where the *bending and twisting* of the 3D manifold attains the memory of the observed co-occurrences of patterns due to object presence. We add additional constraints to the contrastive training, so that the learned distance structure in the latent space captures the pattern correlation that originates from the objects to be discovered. The details will be provided in Section 4.2. We call this latent space a *Pattern Space* that represents all possible patterns in the given image set and their *object-induced associations*.

Another feature of our approach is that diverse backgrounds facilitate estimating correct object boundaries. Our proposed training captures the consistent pattern co-occurrence inside frequent objects, while ignoring accidental co-occurrences due to backgrounds. In typical object recognition problems, the background diversity poses a challenge. In our case, the diversity actually helps by amplifying the correlation within objects and suppressing the accidental correlation between the objects and their background.

4.1 Learning the patch embedding

We train a Variational Autoencoder (VAE) [10] with convolutional layers to learn the embedding, and its architecture is shown in Figure 2. We employ a ResNet-18 backbone plus a global average pooling layer and a fully connected layer generating the latent pattern vector. It is trained from randomly initialized weights. The inputs are the sampled pairs of patches (p_1^i, p_2^i) resized to a standard size of 32×32 . We apply the Sobel filter to the 32×32 patches and feed the gradient images (2 channel

(dx, dy) images) to the training. This serves to reduce the variability of the image patterns, as found effective in [3, 9]. The estimated mean and standard deviation ($z_{\text{mean}}^i, \sigma^i$) =: Encoder(p^i) of the pattern vectors are 100-dimensional each. As in standard VAE training, latent samples are generated by $z^i \sim N(z_{\text{mean}}^i, \sigma^i)$, and are fed to the decoder: Decoder(z^i) := (p^i) ^{\prime} that reconstructs the original patch. The decoder consists of two fully connected layers and four deconvolution layers.

The training loss breaks down to three different losses: (1) contrastive loss, (2) reconstruction loss, and (3) variational KLD loss as used in VAE [10]. As described in the previous subsection, the contrastive loss is the main driver of the self-supervised training. Let $[B] = \{1, \dots, B\}$ where B is the number of images in a batch. The highly overlapping pairs (p_1^i, p_2^i), $i \in [B]$ are the positive examples and the non-overlapping pairs (p_1^i, p_2^j) for $i \neq j$ and $i, j \in [B]$ from different images are the negative examples. The standard Noise Contrastive Estimator (NCE) loss is used to pull matching (IoU > 0.75) pairs close together while pushing non-patching pairs apart.

The NCE loss is designed to maximize the similarity of the positive pair, which is the embedded patches of $z_i = \text{Encoder}(p_i)$ and $z_j = \text{Encoder}(p_j)$. The loss is given by $l_{i,j} = -\text{sim}(z_i, z_j)/\tau + \log \sum_{k=1}^B \mathbf{1}_{[k \neq i]} \exp(\text{sim}(z_i, z_j)/\tau)$, where $\text{sim}(\cdot, \cdot)$ is the cosine similarity between two pattern vectors, and τ is a temperature hyperparameter, following the same approach as in [4, 5].

4.2 Objectness constraints

Even without the presence of objects, the contrastive training will also memorize common background colors and textures in the form of tight latent distance. This is because (1) they often co-occur with objects as backgrounds, (2) they are sampled frequently during training due to their large spatial span, and quite naturally (3) the positive pair of patches sampled from backgrounds tend to be very similar. Blue skies, green fields or forests, and pavements are typical examples. This is not a desirable property for the next step of identifying object boundaries. Our solution is to apply a simple saliency constraint that we call *objectness* to the contrastive loss so that the training is more sensitive to object-like regions rather than their backgrounds. The constraint is enforced by amplifying the contrastive constraint so that the pairs of patches around objects receive tighter ‘pulls’; the contrastive loss is re-weighted by the average objectness score of the pair. The objectness is measured based on two properties: (1) typical objects are tight in spatial span and surrounded by background, and (2) common background patterns span much larger areas than objects and these common patterns often occur in many different images. Figure 2 illustrates our approach for measuring the objectness and modulating the contrastive training. We measure the first property for a potential object using the color histogram difference between the object candidate patch and its surrounding background, denoted by *hscore*. Based on the second property, we developed an effective approach to measure the dissimilarity between a patch and background patterns (which we call ‘*bscore*’). Each of these approaches are detailed in the following subsections.

4.2.1 Histogram distance score

The bounding box of an object has the general property that the color distributions inside and outside of the box are sufficiently different. Based on this property, we measure the objectness by the color histogram difference between either sides of the bounding box. For a given sampled rectangular patch, a boundary band defined by a larger rectangle with its size proportional to the patch size (green rectangular band in Figure 2) captures the hypothetical background pixels. Then these background pixels are converted from RGB to HSV to calculate their H-S (2D) histogram. The same method is applied to the pixels inside the inner rectangle (the original patch) to generate another H-S histogram. The difference between these two histograms represents histogram based object saliency, measured by the Hellinger metric. We call this histogram distance ‘*hscore*’, a histogram based objectness score.

In detail, the $\text{hscore}(p)$ of a patch p is the histogram difference between its inner rectangle p^I and its outer band p^O : $\text{hscore}(p) = d_{\text{Hellinger}}(h(p^I), h(p^O)) - k \cdot \mathbb{E}_{q=q^I \cup q^O, q \in Q} [d_{\text{Hellinger}}(h(q^I), h(q^O))]$, where $h(q)$ is the 2D histogram of the patch q , Q is a collection of all sampled patches. $d_{\text{Hellinger}}(H_1, H_2)$ is the *Hellinger distance* between two histograms: $d_{\text{Hellinger}}(H_1, H_2) = \sqrt{1 - \frac{1}{\sqrt{\bar{H}_1 \bar{H}_2 B^2}} \sum_I \sqrt{H_1(I) \cdot H_2(I)}}$, where $H_1(I)$ and $H_2(I)$ are the frequencies of each bin I , and \bar{H}_1 and \bar{H}_2 are histogram means. The *Hellinger distance*

ranges from value 0 (identical histograms) to 1 (orthogonal histograms). The subtraction by the mean $E[d_{\text{Hellinger}}(\cdot, \cdot)]$ amplifies the effect of modulation. If we use $k = 1$, roughly half of the patch pairs (p_i, p_j) that have lower than average Hellinger distance will have $\text{hscore}(p_i, p_j) < 0$, so that they end up being pushed apart by the contrastive loss. We observed that this causes training to be less stable, thus empirically set the factor at $k = 0.5$ to make it more stable. From each sampled pair of patches p_i and p_j for training, we calculate their average hscore by $\text{hscore}(p_i, p_j) := \frac{1}{2} [\text{hscore}(p_i) + \text{hscore}(p_j)]$ and re-weight the contrastive loss by the average histogram score: $l_{i,j}^{\text{hist}} = \text{hscore}(p_i, p_j) \cdot l_{i,j}$.

4.2.2 Background dissimilarity

After the $\text{hscore}(\cdot)$ re-weigh the contrastive loss, certain background patterns are still detected as candidate objects. This is because these background patterns may co-occur with other structures (such as the space between objects or boundaries of background patterns) and may produce $\text{hscore}(\cdot)$ scores that is not low enough to be discarded. We develop a method that further suppresses these effects by modeling background patterns dominant in a given image set. We identify them by clustering patches in the pixel space, where the patches are randomly sampled from the same image set. Figure 2 shows the procedure. First, these patches are flattened to vectors in $32 \times 32 \times 3$ -dimensional pixel space. We apply the K-means algorithm ($k=5$, empirically determined to capture diverse patterns) to identify the cluster centers as 'typical background patterns'. Then these cluster centers are stored for measuring the $\text{bscore}(p)$ (background similarity score) of any sampled patch p . Given a patch p and the calculated cluster centers c_i of all sampled patches (flattened to vectors by a $\text{vec}(\cdot)$ function), its background distance score $\text{bscore}(p)$ is defined as the distance to the closest background cluster center (the minimum over c_i 's): $\text{bscore}(p) = \min_i \|\text{vec}(p) - c_i\|$. Then the score is normalized by its maximum score among all sampled patches Q : $\text{bscore}^{\text{norm}}(p) = \frac{\text{bscore}(p)}{\text{maxscore}}$, where $\text{maxscore} = \max_{p \in Q} \text{bscore}(p)$.

Finally, the combination of both the hscore and the bscore, by a function $g(\cdot)$, is used to modulate the contrastive loss: $l_{i,j}^{\text{hist}} = g(\text{hscore}(p_i, p_j), \text{bscore}(p_i, p_j)) \cdot l_{i,j}$. We empirically determined that a linear combination of these measures $g(a, b) = k_1 \cdot a + k_2 \cdot b$ (with constants k_1 and k_2) is effective.

5 Object extraction based on clustering pattern vectors

The final step for identifying object boundaries is to cluster the learned pattern vectors, where the clustering is performed over the collection of all pattern vectors sampled from every image in the dataset. The Euclidean distance of a pattern vector to the cluster center, denoted by lscore , is the key measure of the presence of an object within the corresponding patch. We also found it beneficial to add both the histogram distance based objectness score hscore and the background similarity score bscore to the cluster distance. We call this P-O (*Post-Objectness*) constraint and we will validate its usefulness in the experimental sections. Here is the summary of the procedure:

Algorithm 1: Object extraction

1. Fixed number (200) of patches are sampled from each image in the dataset, and combined into a single pool of patches.
 2. The trained pattern space embedding maps all the patches to pattern vectors.
 3. 1-mean clustering determines their center and each vector's distance lscore to the center.
 4. P-O (Post-Objectness) constraint: Both the $1 - \text{hscore}$ and $1 - \text{bscore}$ are calculated and added to the lscore to calculate the final score: $\text{score} = \text{lscore} + \alpha_h \cdot (1 - \text{hscore}) + \alpha_b \cdot (1 - \text{bscore})$, where α_h and α_b are constants (empirically set as $\alpha_h = \alpha_b = \text{average}(\text{lscore}) \approx 5.0$).
 5. For each image, the patches that output lower scores are selected as object candidates. $N_{\text{candidate}} = 20$ low score patches are selected per image after being sorted by the scores.
 6. Non-maxima suppression is applied to the selected candidate patches and final patches are selected as the discovered objects, with the overlap threshold of 0.5. Maximum of $N_{\text{predict}} = 5$ patches per image are selected as object candidates.
-

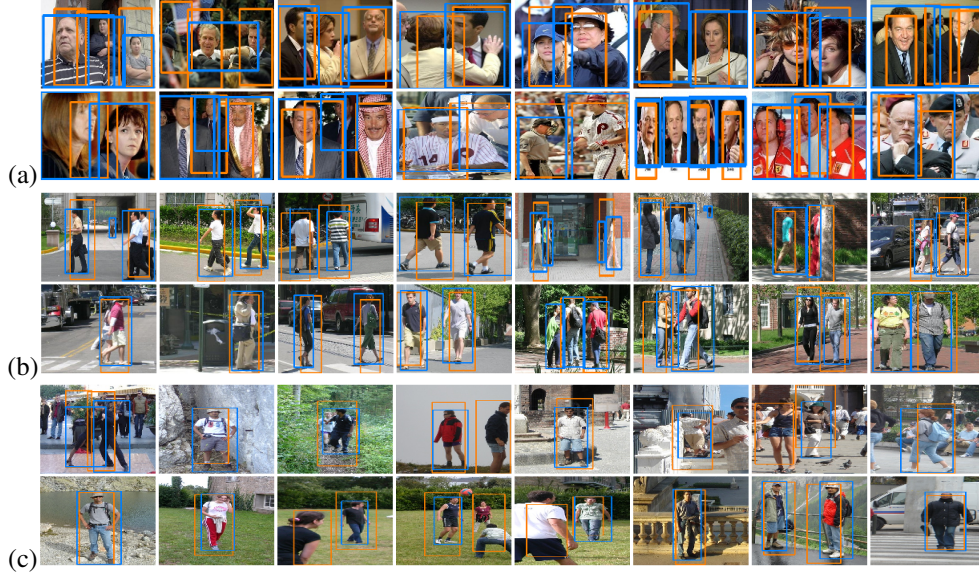


Figure 3: Object discovery results to (a) Fddb100, (b) Penn-Fudan, and (c) INRIA-EZ datasets

6 Experimental results

6.1 Datasets and visual results

Fddb-100 dataset¹ is a subset of the LFW dataset² that consists of 5,171 annotated faces in a set of 2,845 images, constructed for face detection research. We selected the first 100 images from Fddb to test the object discovery performance. We do not use the original facial bounding box annotations, but person level annotations as ground truth. This is because our approach picks up any common visible patterns in the image, and that includes body portions outside of faces. Figure 3 shows the images and the discovered bounding boxes (color coded in orange) compared to the ground truth (color coded in blue). The bounding boxes are not localized with high accuracy, but able to resolve multiple people based on object (person) representation learned from merely 100 images.

Penn-Fudan dataset³ consists of pedestrian images taken around campus and urban streets. It has 170 images with 345 labeled pedestrians, among which 96 images are taken from around University of Pennsylvania, and other 74 are taken from around Fudan University. Figure 3 shows the images and the ground truth & discovered bounding boxes marked with the same color scheme.

INRIA-EZ dataset is a subset of the well-known INRIA person dataset⁴. The INRIA dataset consists of 902 images (both Train and Test images) that contain images of people against diverse scenes such as streets, tourist attractions, parks, beaches, mountains, trade shows, etc. We have selected images and objects that are less challenging for detection. The selection criteria are: (1) image having five or less people and (2) ground truth bounding boxes larger than 10K pixels (roughly 60x180 bounding box) within these selected images. These two criteria led to 205 images with 272 ground truth bounding boxes of people. Figure 3 shows the images and object discovery results. (Object discovery outputs from all images from three datasets are in the supplementary material.)

6.2 Metric evaluation results

We use two performance metrics for measuring the success of object discovery. For evaluating single-object discovery, we use a metric frequently used in similar object discovery contexts [6, 23, 24] called correct localization (CorLoc), which is defined as the percentage of images that our model

¹<http://vis-www.cs.umass.edu/fddb/>

²<http://vis-www.cs.umass.edu/lfw/>

³https://www.cis.upenn.edu/~jshi/ped_html/

⁴<http://pascal.inrialpes.fr/data/human/>

Modes		FDDDB100				PennFudan				INRIA-EZ			
Modulation	Post-Obj	Corloc	Recall	Precision	F1	Corloc	Recall	Precision	F1	Corloc	Recall	Precision	F1
x	x	70.30	53.10	54.33	53.70	63.12	35.56	23.08	27.99	55.17	51.91	17.54	26.22
		± 2.15	± 2.31	± 2.65	± 2.42	± 2.11	± 1.56	± 1.08	± 1.26	± 2.71	± 2.79	± 0.97	± 1.44
x	✓	70.60	54.21	56.08	55.12	69.76	38.63	27.33	32.01	56.39	52.39	22.65	31.62
		± 2.54	± 2.90	± 3.00	± 2.89	± 3.64	± 1.58	± 1.10	± 1.27	± 3.46	± 3.31	± 1.53	± 2.10
✓	x	70.20	54.00	55.05	54.51	69.00	37.21	23.99	29.17	57.85	54.26	19.09	28.24
		± 3.19	± 3.52	± 3.78	± 3.60	± 2.67	± 0.96	± 0.81	± 0.88	± 4.04	± 3.89	± 1.39	± 2.04
✓	✓	70.30	54.21	54.70	54.44	74.00	39.69	29.23	33.66	51.71	47.48	27.64	34.94
		± 2.90	± 2.21	± 1.89	± 1.98	± 3.67	± 1.85	± 1.25	± 1.48	± 2.48	± 2.07	± 1.23	± 1.54

Table 1: Metric evaluation results for $iou_{\text{thres}} = 0.5$

correctly localized at least one target object. The localization accuracy is measured by the common IoU (intersection over union) computation. An IoU over 0.5 ($iou_{\text{thres}} = 0.5$) is regarded as success in most of our evaluations, and we consider a relaxed criterion of $iou_{\text{thres}} = 0.4$ as well. For measuring accuracy of multi-object discovery, traditional detection metrics based on Precision and Recall scores also apply. However, we found that AP (Average Precision) is not suitable. In supervised learning scenarios, the detection scores are estimated from the ground truth object presence in each image and at each position. Therefore they provide a decision score consistent across images and within each image. However, our measure of object presence based cluster distance lacks the same consistency and does not interpret directly as a detection score. We use the F1 score for combining recall and precision for our evaluation. The F1 score is developed for measuring the success of information retrieval, and finding an object among randomly generated patches can be regarded as a retrieval problem. Just as the AP is averaged over the range of recall values by varying the detection score threshold, we can control the number of maximum predictions per image to sweep the (recall, precision) ranges. Then we identify the maximum of F1 scores over the range of number of max predictions (from 1 to 5) as the reported accuracy. We also report CorLoc, recall, and precision scores measured at the maximum F1 score. Because the candidate patches are randomly generated, the metric numbers are averaged over ten iterations and their error bounds in terms of standard deviations are listed as \pm STD.

The first set of experiments confirm the benefits of the contrastive loss modulation and the P-O constraints. Table 1 summarizes the accuracy metrics over different combinations of these features. For the two pedestrian datasets, the modulated contrastive training combined with the P-O constraints (both the histogram and background constraints) achieves the overall best performance compared to other modes. The modulated contrastive training (third and fourth rows vs. first and second rows) clearly demonstrates that the loss modulation improves accuracy regardless of the P-O constraints. On the other hand, the effect of the P-O constraint (first vs. second and third vs. fourth) appears more significant. The FDDDB-100 dataset seems to enjoy less benefit from either features. We suspect this is due to many images occupied mostly by faces or bodies (often overlap with other people) without clear boundaries against the background. However, these features do not hurt the accuracy either. We conclude that the combination of both the modulated training and the P-O constraint achieves overall the best accuracy.

Modes		FDDDB100				Penn-Fudan				INRIA-EZ			
Modulation	Post-Obj	Corloc	Recall	Precision	F1	Corloc	Recall	Precision	F1	Corloc	Recall	Precision	F1
x	✓	88.20	72.69	74.81	73.73	86.47	53.92	38.23	44.74	70.39	65.65	37.49	47.72
		± 1.47	± 2.21	± 1.84	± 1.91	± 2.10	± 2.07	± 1.75	± 1.90	± 2.19	± 1.91	± 1.08	± 1.37
✓	✓	87.80	72.69	73.25	72.96	88.35	53.59	39.22	45.29	73.37	67.30	38.99	49.38
		± 1.72	± 2.12	± 3.02	± 2.44	± 1.62	± 1.99	± 1.00	± 1.35	± 2.74	± 2.28	± 1.30	± 1.65

Table 2: Metric evaluation results for $iou_{\text{thres}} = 0.4$

The next experiments test a relaxed detection criterion. Our approach does not utilize ground truth bounding boxes, but rather find emergent patterns from images. Therefore the bounding box estimates are often not accurate. We find many cases where bounding boxes appear to originate from true objects, evidenced by many loose bounding boxes around objects when objects are well separated. For this reason, we report the accuracy results based on the matching criteria of $IoU > 0.4$ as another legitimate success measure to guide our study. The results are reported in Table 2. We only selected (1) contrastive training with P-O constraints and (2) modulated training with P-O constraints, since

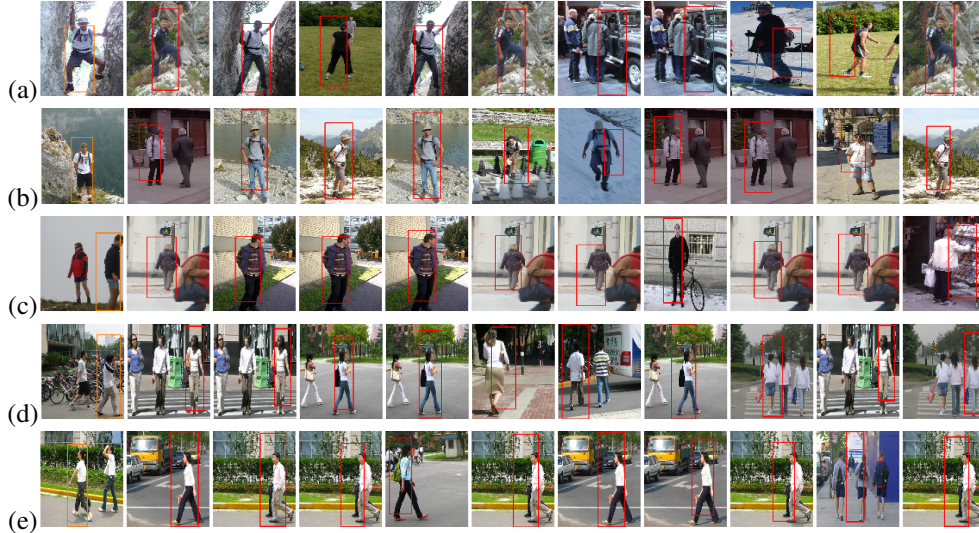


Figure 4: Discovered objects and their closest neighbors in latent space

we confirmed their benefit from the previous experiments. The accuracy numbers show significant gain, and the benefit of the modulated training is confirmed again for the two pedestrian datasets.

We also confirm the effectiveness of the background based objectness toward images having common backgrounds. Table 3 summarizes accuracy numbers (only F1 for clear comparison) from different modes: P-O is turned on but modulation by histogram only, or background only, or both. Penn-Fudan data is collected from two campuses therefore the background scenes are limited. The F1 score clearly shows that the bscore based modulation greatly benefits object discovery from Penn-Fudan images.

6.3 Latent neighbor analysis

Modulation		FDDB100		Penn-Fudan		INRIA-EZ	
Hist.	Bgnd.	F1	std	F1	std	F1	std
x	x	55.12	±2.89	32.01	±1.27	31.62	±2.10
✓	x	58.31	±1.91	32.77	±1.70	34.12	±1.16
x	✓	56.62	±3.90	34.44	±1.25	34.62	±1.71
✓	✓	54.44	±1.98	33.66	±1.48	34.94	±1.54

Table 3: Modulation by histogram vs background vs both

Table 3: Modulation by histogram vs background vs both

appear to show common background textures while all rows show consistent body poses. The nearest neighbors also capture similar clothing (c, d, and e) and backpacks people wear (b). However, the analysis is only based on distance, and we have not developed further training constraints or analysis tools to enforce and discover disentangled visual features.

Conclusion

We demonstrated that self-supervised training of randomly generated patches modulated by objectness constraints finds common object patterns from relatively small number of images quite effectively. One of its major limitations is the low localization accuracy and this topic is our active focus of investigation. Another desirable feature is to identify multiple classes of objects from a single unsupervised training. We suspect that combination with Deep Clustering approaches [3, 9, 22] may enable multi-class object discovery based on contrastive training. Another avenue is to make the proposed object discovery more practical by incorporating minimal supervision.

References

- [1] Hakan Bilen and Andrea Vedaldi. Weakly supervised deep detection networks. In *2016 IEEE Conference on Computer Vision and Pattern Recognition (CVPR)*, pages 2846–2854, 2016.
- [2] Christopher P. Burgess, Loic Matthey, Nicholas Watters, Rishabh Kabra, Irina Higgins, Matt Botvinick, and Alexander Lerchner. Monet: Unsupervised scene decomposition and representation, 2019.
- [3] Mathilde Caron, Piotr Bojanowski, Armand Joulin, and Matthijs Douze. Deep clustering for unsupervised learning of visual features. In *Proceedings of the European Conference on Computer Vision (ECCV)*, pages 132–149, 2018.
- [4] Ting Chen, Simon Kornblith, Mohammad Norouzi, and Geoffrey Hinton. A simple framework for contrastive learning of visual representations. *Proceedings of the International Conference on Machine Learning (ICML)*, 2020.
- [5] Ting Chen, Simon Kornblith, Kevin Swersky, Mohammad Norouzi, and Geoffrey E Hinton. Big self-supervised models are strong semi-supervised learners. *Advances in Neural Information Processing Systems*, 33, 2020.
- [6] Minsu Cho, Suha Kwak, Cordelia Schmid, and Jean Ponce. Unsupervised object discovery and localization in the wild: Part-based matching with bottom-up region proposals. In *2015 IEEE Conference on Computer Vision and Pattern Recognition (CVPR)*, pages 1201–1210, 2015.
- [7] Martin Engelcke, Adam R. Kosior, Oivi Parker Jones, and Ingmar Posner. Genesis: Generative scene inference and sampling with object-centric latent representations, 2019.
- [8] Klaus Greff, Raphaël Lopez Kaufman, Rishabh Kabra, Nick Watters, Christopher Burgess, Daniel Zoran, Loic Matthey, Matthew Botvinick, and Alexander Lerchner. Multi-object representation learning with iterative variational inference. In Kamalika Chaudhuri and Ruslan Salakhutdinov, editors, *Proceedings of the 36th International Conference on Machine Learning*, volume 97 of *Proceedings of Machine Learning Research*, pages 2424–2433. PMLR, 09–15 Jun 2019.
- [9] Xu Ji, Joao F. Henriques, and Andrea Vedaldi. Invariant information clustering for unsupervised image classification and segmentation. In *Proceedings of the IEEE/CVF International Conference on Computer Vision (ICCV)*, October 2019.
- [10] Diederik P Kingma and Max Welling. Auto-encoding variational bayes. *arXiv preprint arXiv:1312.6114*, 2013.
- [11] Xiaoyan Li, Meina Kan, Shiguang Shan, and Xilin Chen. Weakly supervised object detection with segmentation collaboration. In *2019 IEEE/CVF International Conference on Computer Vision (ICCV)*, pages 9734–9743, 2019.
- [12] Wei Liu, Dragomir Anguelov, Dumitru Erhan, Christian Szegedy, Scott Reed, Cheng-Yang Fu, and Alexander C Berg. Ssd: Single shot multibox detector. In *European conference on computer vision*, pages 21–37. Springer, 2016.
- [13] Francesco Locatello, Dirk Weissenborn, Thomas Unterthiner, Aravindh Mahendran, Georg Heigold, Jakob Uszkoreit, Alexey Dosovitskiy, and Thomas Kipf. Object-centric learning with slot attention. In H. Larochelle, M. Ranzato, R. Hadsell, M. F. Balcan, and H. Lin, editors, *Advances in Neural Information Processing Systems*, volume 33, pages 11525–11538. Curran Associates, Inc., 2020.
- [14] Santiago Manen, Matthieu Guillaumin, and Luc Van Gool. Prime object proposals with randomized prim’s algorithm. In *2013 IEEE International Conference on Computer Vision*, pages 2536–2543, 2013.
- [15] Sai Saketh Rambhatla, Rama Chellappa, and Abhinav Shrivastava. The pursuit of knowledge: Discovering and localizing novel categories using dual memory, 2021.
- [16] Joseph Redmon, Santosh Divvala, Ross Girshick, and Ali Farhadi. You only look once: Unified, real-time object detection. In *Proceedings of the IEEE conference on computer vision and pattern recognition*, pages 779–788, 2016.
- [17] Zhongzheng Ren, Zhiding Yu, Xiaodong Yang, Ming-Yu Liu, Yong Jae Lee, Alexander G. Schwing, and Jan Kautz. Instance-aware, context-focused, and memory-efficient weakly supervised object detection. In *Proceedings of the IEEE/CVF Conference on Computer Vision and Pattern Recognition (CVPR)*, June 2020.

- [18] Peng Tang, Xinggang Wang, X. Bai, and Wenyu Liu. Multiple instance detection network with online instance classifier refinement. *2017 IEEE Conference on Computer Vision and Pattern Recognition (CVPR)*, pages 3059–3067, 2017.
- [19] Peng Tang, Xinggang Wang, Angtian Wang, Yongluan Yan, Wenyu Liu, Junzhou Huang, and Alan Yuille. Weakly supervised region proposal network and object detection. In Vittorio Ferrari, Martial Hebert, Cristian Sminchisescu, and Yair Weiss, editors, *Computer Vision – ECCV 2018*, pages 370–386, Cham, 2018. Springer International Publishing.
- [20] Jasper RR Uijlings, Koen EA Van De Sande, Theo Gevers, and Arnold WM Smeulders. Selective search for object recognition. *International journal of computer vision*, 104(2):154–171, 2013.
- [21] Wouter Van Gansbeke, Simon Vandenhende, Stamatios Georgoulis, Marc Proesmans, and Luc Van Gool. Scan: Learning to classify images without labels. In *European Conference on Computer Vision*, pages 268–285. Springer, 2020.
- [22] Pascal Vincent, Hugo Larochelle, Yoshua Bengio, and Pierre-Antoine Manzagol. Extracting and composing robust features with denoising autoencoders. In *Proceedings of the 25th international conference on Machine learning*, pages 1096–1103, 2008.
- [23] Huy V. Vo, Francis Bach, Minsu Cho, Kai Han, Yann LeCun, Patrick Perez, and Jean Ponce. Unsupervised image matching and object discovery as optimization. In *Proceedings of the IEEE/CVF Conference on Computer Vision and Pattern Recognition (CVPR)*, June 2019.
- [24] Huy V. Vo, Patrick Pérez, and Jean Ponce. Toward unsupervised, multi-object discovery in large-scale image collections. In Andrea Vedaldi, Horst Bischof, Thomas Brox, and Jan-Michael Frahm, editors, *Computer Vision – ECCV 2020*, pages 779–795, Cham, 2020. Springer International Publishing.
- [25] Xiaolong Wang, Abhinav Shrivastava, and Abhinav Gupta. A-fast-rcnn: Hard positive generation via adversary for object detection. In *Proceedings of the IEEE conference on computer vision and pattern recognition*, pages 2606–2615, 2017.
- [26] Xiu-Shen Wei, Chen-Lin Zhang, Jianxin Wu, Chunhua Shen, and Zhi-Hua Zhou. Unsupervised object discovery and co-localization by deep descriptor transformation. *Pattern Recognition*, 88:113–126, 2019.
- [27] Runsheng Zhang, Yaping Huang, Mengyang Pu, Jian Zhang, Qingji Guan, Qi Zou, and Haibin Ling. Object discovery from a single unlabeled image by mining frequent itemsets with multi-scale features. *IEEE Transactions on Image Processing*, 29:8606–8621, 2020.